

QSW_MPI: a framework for parallel simulation of quantum stochastic walks

Edric Matwiejew^{a,*}, Jingbo Wang^a

^a*Department of Physics, The University of Western Australia, Perth, Australia*

Abstract

QSW_MPI is a python package developed for the modeling of quantum stochastic walks, a generalization of the classical random walk and continuous-time quantum walk in the Lindblad formalism. This model allows for the study of a wide range of Markovian open quantum systems subject to varying degrees of incoherent scattering. Consisting of a python interface built on parallelized Fortran libraries utilizing sparse data structures; QSW_MPI is scalable to massively parallel computers, making possible the simulation of walks on graphs with many thousands of vertices. QSW_MPI also provides explicit support for an extension of the standard quantum stochastic walk model to the study of non-Hermitian absorption and emission processes.

Keywords: quantum stochastic walk, Markovian open systems, Lindblad master equation, parallel computation

PROGRAM SUMMARY

Program Title: QSW_MPI

Licensing provisions: GPLv3

Programming language: Python 3 + Fortran 2003

Computer and operating system: Systems supporting python 3 and an MPI implementation.

RAM: 16 GB minimum recommended, memory requirements scale with graph size and connectivity.

Number of processors used: Arbitrary number of processors supported via MPI.

Classification: 4.15 Quantum Computing, 6.5 Software including Parallel Algorithms

External routines/libraries: NumPy [1], SciPy [2], mpi4py [3], NetworkX [4], Matplotlib [5], h5py [6]

Nature of problem:

QSW_MPI provides a framework for the simulation of quantum stochastic walks on arbitrary graphs (directed/undirected, weighted/unweighted) incorporating absorption and emission processes.

Solution method:

A parallel distributed meory implementation of the matrix exponential via a truncated Taylor series expansion with scaling and squaring.

Restrictions:

QSW_MPI will provide support for the simulation of multiple quantum walkers in a future version.

References

- [1] T. Oliphant, NumPy: A guide to NumPy, 2006, published: USA: Trelgol Publishing.
- [2] E. Jones, T. Oliphant, P. Peterson, SciPy: Open source scientific tools for Python (2001).
- [3] L. Dalcin, R. Paz, M. Storti, J. D'Elia, MPI for Python: Performance improvements and MPI-2 extensions, *Journal of Parallel and Distributed Computing* 68 (5) (2008) 655662. doi:10.1016/j.jpdc.2007.09.005.
- [4] A. A. Hagberg, D. A. Schult, P. J. Swart, Exploring Network Structure, Dynamics, and Function using NetworkX, in: G. Varoquaux, T. Vaught, J. Millman (Eds.), *Proceedings of the 7th Python in Science Conference*, Pasadena, CA USA, 2008, pp. 11–15.
- [5] J. D. Hunter, Matplotlib: A 2d graphics environment, *Computing in Science & Engineering* 9 (3) (2007) 9095. doi:10.1109/MCSE.2007.55.
- [6] A. Collette, *Python and HDF5*, O'Reilly, 2013.

1. Introduction

The exploration of nanoscale systems and quantum information are at the core of a new generation of technologies, including quantum computation and molecular-scale electronics. This necessitates the development of efficient simulation software capable of modelling the dynamics of these systems in their practical application i.e. when subject to decoherence. To this effort we have developed QSW_MPI [1]; a package designed for the efficient simulation of Quantum Stochastic Walks (QSWs) on both workstations and massively parallel computers.

Walk based models describe the probabilistic evolution of a system consisting of discrete sites linked by a coupling potential, which together constitute a network (or graph). These include the Continuous-Time Random Walk (CTRW) and its quantum analogue, the Continuous-Time Quantum Walk (CTQW). Such models have been applied to a wide range of physical and informatic systems. For example, their natural correspondence to the tight binding model in solid state physics has seen their application to the study of quantum and classical energy transport in molecular systems [2, 3]. Elsewhere in the rapidly developing field of quantum computing, quantum-walk based algorithms have been developed which are exponentially faster than their classical counterparts.

Developed by Whitfield *et al.* in 2010, QSWs described a quantum walk subject to an external environment, whose decohering effects are derived axiomatically from the underlying network. The result of this is a generalization of the CTRW

*Corresponding author.

E-mail address: Edric.Matwiejew@research.uwa.edu.au

and CTQW, which allows for the exploration of dynamics in a continuum from the quantum to classical regimes.

Since their introduction, QSWs have been implemented experimentally [4], a recent example being their application to the design of artificial neurons [5]. They have also been explored as a basis for quantum algorithms. A QSW-based variant of the PageRank search engine algorithm exhibited final distributions which broke undesirable degeneracies present in the classical version, while also speeding up the rate of convergence [6, 7].

One of the most notable applications has been the use of QSWs to describe quantum assisted transport through the light harvesting complexes of photosynthetic bacteria [8]. This extended the QSW model to include the non-unitary processes of absorption into and emission from the network. These processes have since been formally introduced to the QSW model and applied to the study of transport in monomers, dimers and topologically disordered networks [9].

The established expressiveness and flexibility of the QSW model thus motivates making possible its application to systems of greater complexity. To this end, software packages for the simulation of QSWs have been developed using Mathematica and the Julia programming language [10, 11] [12]. They both offer a user friendly interface, but are limited in the simulated network size due to memory constraints and their reliance on single-process linear algebra libraries.

QSW_MPI addresses these limitations by taking a distributed memory approach to the construction of the QSW superoperator and the calculation of the system evolution via matrix exponentiation. This takes the form of subroutines contained in Fortran libraries with which the user interacts using a python interface; taking advantage of the ubiquity of the interpreted python language and the speed afforded by highly optimized Fortran compilers. This allows a user to write simulations appropriate for execution on massively parallel computers with minimal background in programming or parallel computation. An additional novel feature of this package is its explicit support for the inclusion of absorption and emission process through easily defined modifications to the underlying network structure.

This paper thus proceeds as follows. In Section 2 the mathematical framework of QSWs is introduced, along with its extension to the modeling of non-Hermitian transport processes. Section 3 provides an overview of the computational methods utilized in QSW_MPI. This is followed by an overview of the software package, with particular attention given to its installation and usage. Validation and performance of the QSW_MPI is discussed in Section 5, and concluding statements given in Section 6.

2. Theory

This section provides a self-contained overview of the mathematical formalism underpinning a QSW. The starting point of this is the definition of the CTRW and CTQW on networks, followed by an overview of the master equation approach to the description of Markovian open systems. From this the QSW

master equation is then introduced, which unifies the CTRW and CTQW models under a density theoretic framework. The practical extension of this equation to the inclusion of non-Hermitian absorption and emission process is then discussed. We conclude by presenting the vectorized form of the QSW master equation. This produces a structurally simplified form of the Master equation, the numerical approximation of which is the task at hand.

2.1. Networks

A network (or ‘graph’) is defined as an object $\mathcal{G} = (E, V)$ comprised of $V = \{1, \dots, N\}$ vertices (or ‘sites’) connected by a set of edges $E = \{i \rightarrow j, k \rightarrow l, \dots\}$. This is represented by an $N \times N$ adjacency matrix, G ,

$$G_{ij} = \begin{cases} G_{ij} > 0, & \exists(i \rightarrow j) \\ 0, & \text{otherwise} \end{cases} \quad (1)$$

where $G_{ij} \in \mathbb{R}$ describes the magnitude of connection between two vertices i and j [10]. Edges of form A_{ii} are known as self loops with a graph containing no self loops being referred to as a ‘simple’ graph. The case where $A_{ij} \neq A_{ji}$ encodes directionality into the graph structure, such graphs being referred to as ‘directed’. Conversely, graphs for which all $A_{ij} = A_{ji}$ are referred to as ‘undirected’. The sum total of the outgoing edge weights from vertex j ,

$$\text{outDeg}(j) = \sum_{i \neq j} G_{ij} \quad (2)$$

is termed the vertex ‘out degree’[10].

2.2. Continuous-Time Classical Random Walks

A CTRW describes the probabilistic evolution of a system (walker) through a parameter space as a continuous function of time [9]. Most typically, CTRWs refer to a type of Markov process. This describes a scenario where the future state of a system depends only on its current state. Heuristically, one might describe such systems as having a ‘short memory’. Under this condition a CTRW over a network is described by a system of first order ordinary differential equations,

$$\frac{d\vec{p}(t)}{dt} = -M\vec{p}(t) \quad (3)$$

where element $p_i \geq 0$ of $\vec{p}(t)$ is the probability of the walker being found at vertex i of the network, and $\vec{p}(t)$ has the solution $\vec{p}(t) = \exp(-tM)\vec{p}(0)$ which satisfies $\sum \vec{p}(t) = 1$ [13]. M is the transition matrix derived from G ,

$$M_{ij} = \begin{cases} -\gamma G_{ij}, & i \neq j \\ \gamma \text{outDeg}(j), & i = j \end{cases} \quad (4)$$

where the off-diagonal elements M_{ij} represent the probability flow along an edge from vertex j to vertex i , while the diagonal elements M_{jj} account for the total outflow from vertex j per unit time. Scalar $\gamma \in \mathbb{R}$ is the system wide network transition rate [10].

2.3. Continuous-Time Quantum Walks

A Continuous-Time Quantum Walk (CTQW) is constructed by mapping \mathcal{G} to an N -dimensional Hilbert space where the set of its vertices $\{|1\rangle, \dots, |N\rangle\}$ form an orthonormal basis. The matrix elements of the system Hamiltonian H are then equal to the classical transition matrix $(\langle i|H|j\rangle = M_{ij})$. In place of $\vec{p}(t)$, the evolution of the state vector $|\Psi(t)\rangle = \sum_{i=1}^N |i\rangle \langle i|\Psi(t)\rangle$ is considered, the dynamics of which are governed by the Schrödinger equation [10],

$$\frac{d|\Psi(t)\rangle}{dt} = -\frac{i}{\hbar} H |\Psi(t)\rangle \quad (5)$$

which has the formal solution $|\Psi(t)\rangle = \exp(-itH) |\Psi(0)\rangle$ when H is time-independent¹. The probability associated with vertex i at time t is then given by $|\langle i|\Psi(t)\rangle|^2$.

While Equations 3 and 5 appear superficially similar, there are a number of fundamental differences between the two processes. Firstly, $|\Psi(t)\rangle$ describes a complex probability amplitude, meaning that its possible paths may interfere. Secondly, the Hermiticity requirement on H needed to maintain unitary (probability preserving) evolution of the system dictates that \mathcal{G} must be an undirected graph [9, 10].

2.4. Markovian Open Quantum Systems

A density matrix,

$$\rho(t) = \sum_k p_k |\Psi_k(t)\rangle \langle \Psi_k(t)|, \quad (6)$$

describes a statistical ensemble of quantum states, $|\Psi_k(t)\rangle$, each with an associated probability $p_k \geq 0 \in \mathbb{R}$ and $\sum_k p_k = 1$. The case where p_k is non-zero for more than one k is termed a ‘mixed state’ while the case of only one non-zero p_k is termed a ‘pure state’.

Density matrices satisfy: $\rho(t)^\dagger = \rho(t)$, $\text{tr}\{\rho(t)\} = 1$, $\text{trace}(\rho(t)^2) \leq 1$ (with equality holding for only pure states) and $\langle A \rangle = \text{trace}(\rho(t)A)$ (where A is a quantum operator) [10]. Diagonal elements ρ_{ii} represent the probability density at a given vertex and are termed ‘populations’, while off-diagonal elements ρ_{ij} describe phase coherence between vertices i and j .

The dynamics of $\rho(t)$ are given by the Liouville-von Neumann equation,

$$\frac{d\rho(t)}{dt} = -i[H, \rho(t)], \quad (7)$$

which is the density theoretic equivalent of the Schrödinger equation (Equation 5) [14].

Consider a system, S , coupled to an external reservoir (or ‘bath’), B . The Hilbert space of $S + B$ is given by [14],

$$\mathcal{H} = \mathcal{H}_S \otimes \mathcal{H}_B, \quad (8)$$

where \mathcal{H}_S and \mathcal{H}_B are the Hilbert spaces of S and B . S is referred to as an ‘open’ system, while $S + B$ is closed in the

sense that its dynamics can be described unitarily. Under the conditions that the evolution of S is Markovian with no correlation between S and B at $t = 0$, and given \mathcal{H}_S of finite dimensions N . The dynamics of S are described by a generalization of Equation 7: the Kossakowski-Lindblad quantum master equation [14],

$$\frac{d\rho_S(t)}{dt} = -\frac{i}{\hbar} [H, \rho_S(t)] + \sum_{k=1}^{N^2} \tau_k (L_k \rho_S(t) L_k^\dagger - \frac{1}{2} \{L_k^\dagger L_k, \rho_S(t)\}) \quad (9)$$

where H is not necessarily H_S as it may incorporate unitary dynamics in both S and B ; the Lindblad operators L_k span the Liouville space and the scalars $\tau_k \geq 0 \in \mathbb{R}$. The reduced density operator $\rho(t)_S$ is formed by tracing out the degrees of freedom associated with B . Equation 9 is invariant under unitary transformations of the Lindblad operators, allowing for construction of a wide range of phenomenological models [9].

It is useful to introduce the shorthand,

$$\mathcal{D}_k[\rho_S(t)] = \tau_k (L_k \rho_S(t) L_k^\dagger - \frac{1}{2} \{L_k^\dagger L_k, \rho_S(t)\}), \quad (10)$$

which are referred to as a ‘dissipator’. Inclusion of these terms results in decoherence and relaxation effects in the dynamics of $\rho_S(t)$, observed mathematically as decay in the off-diagonal coherences of $\rho_S(t)$ to zero with sufficient t . Importantly, this has the following consequence: processes obeying the master equation have a well defined equilibrium state, which is not the case for unitary dynamics [9].

2.5. Quantum Stochastic Walks

2.5.1. Standard Definition

A QSW on a graph is derived from Equation 10 by defining $\rho_s(t)$ in the basis of vertex states, $\{|1\rangle, \dots, |N\rangle\}$, and constructing a unitary Hamiltonian from the adjacency matrix, G , of an arbitrary \mathcal{G} ,

$$H_{ij} = \begin{cases} -\gamma \max(G_{ij}, G_{ji}), & i \neq j \\ \gamma \text{outDeg}(j), & i = j \end{cases} \quad (11)$$

and the Lindblad operators from its transition matrix M (Equation 4),

$$L_k = \sqrt{|M_{ij}|} |i\rangle \langle j|. \quad (12)$$

where $k = N(j-1) + i$. Each L_k then describes an incoherent scattering channel along a directed graph edge. Importantly, this allows for the encoding of directness resulting from the edge weights of \mathcal{G} into the walk’s dynamics [10].

Finally, a scalar decoherence parameter $0 \leq \omega \leq 1$ is introduced [15]. This allows for the model to be easily tuned to explore a continuum of mixed quantum and classical dynamics. The standard form of a QSW is then,

$$\frac{d\rho(t)}{dt} = -i(1-\omega)[H, \rho(t)] + \omega \sum_{k=1}^{N^2} \mathcal{D}_k[\rho(t)] \quad (13)$$

¹In atomic units where $\hbar = 1$ a.u = $1.054\,571 \times 10^{-34}$ J.s and $t = 2.418884 \times 10^{-17}$ s = 24.188 84 fs.

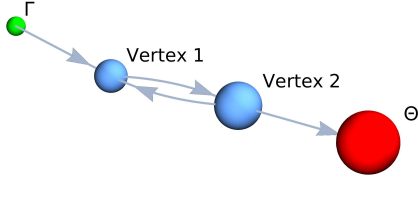


Figure 1: A dimer graph with a source (Γ) attached to vertex 1 and a sink (Θ) attached to vertex 2. Note that the absorption and emission channels are unidirectional.

with $\rho_s(t)$ denoted as $\rho(t)$ and $\tau_k = \omega$ for all dissipator terms. At $\omega = 0$, Equation 13 reduces to a CTQW obeying the Liouville-von Neumann equation (Equation 7) and, at $\omega = 1$, the density-matrix equivalent of the CTRW equation (Equation 3) is obtained.

2.5.2. Extension to Absorption and Emission

The QSW model naturally facilitates the modelling of absorption and emission processes through the inclusion of Lindblad operators describing scattering channels that do not have a counterpart in the coherent Hamiltonian. The addition of these dynamics to the QSW framework have been derived formally [9]. With the QSW operators in their matrix representations, this is practically achieved by forming the Lindblad operators from an augmented adjacency matrix, G_{aug} , containing G and the additional channels as non-symmetric edge weights. Here, the absorption channels (sources) are,

$$G_\Gamma = \{\Gamma_k \subset G_{\text{aug}} : i > N, j \leq N\} \quad (14)$$

and emission channels (sinks),

$$G_\Theta = \{\Theta_k \subset G_{\text{aug}} : i \leq N, j > N\}, \quad (15)$$

where $k = \tilde{N}(j-1) + i$ with \tilde{N} equal to N plus the total number of sources and sinks, and $\Gamma_k > 0 \in \mathbb{R}$ is the absorption rate at vertex j and $\Theta_k > 0 \in \mathbb{R}$ is the emission rate at vertex i . A vertex in the non-augmented network to which a source is attached is referred to as an absorption vertex, while a vertex to which an emission channel is attached is referred to as an emission vertex.

For example, consider a dimer graph shown in Figure 1 on which absorption is modeled at vertex 1 ($\Gamma_9 = 2$) and emission at vertex 2 ($\Theta_8 = 3$). The corresponding QSW has H formed by adjacency matrix G , the unaugmented 2×2 adjacency padded to maintain dimensional consistency, and its Lindblad operators derived from G_{aug} , where

$$G = \begin{bmatrix} 0 & 1 & 0 & 0 \\ 1 & 0 & 0 & 0 \\ 0 & 0 & 0 & 0 \\ 0 & 0 & 0 & 0 \end{bmatrix}, \quad G_{\text{aug}} = \begin{bmatrix} 0 & 1 & 2 & 0 \\ 1 & 0 & 0 & 0 \\ 0 & 0 & 0 & 0 \\ 0 & 3 & 0 & 0 \end{bmatrix}. \quad (16)$$

As such, a QSW incorporating both absorptive and emissive processes can be succinctly expressed as,

$$\begin{aligned} \frac{d\rho(t)}{dt} = & -i(1-\omega)[H, \rho(t)] \\ & + \omega \sum_{k \in G}^{N^2} \mathcal{D}_k[\rho(t)] \\ & + \sum_{k \in G_\Gamma} \Gamma_k \mathcal{D}_k[\rho(t)] \\ & + \sum_{k \in G_\Theta} \Theta_k \mathcal{D}_k[\rho(t)] \end{aligned} \quad (17)$$

with $\rho(t)$ being of dimensions $\tilde{N} \times \tilde{N}$.

2.5.3. Vectorization of the Master Equation

Equation 17 may be recast as a system of first order differential equations through its representation in a $\tilde{N}^2 \times \tilde{N}^2$ Liouville space [14]. This process, termed ‘Vectorization’, makes use of the identity $\text{vec}(X \cdot Y \cdot Z) = (Z^T \otimes X)$ to obtain a form of the QSW master equation consisting of a linear sum in its Hamiltonian and Lindblad operators. Meaning that its equation of motion,

$$\frac{d\tilde{\rho}(t)}{dt} = \tilde{\mathcal{L}} \cdot \tilde{\rho}(t) \quad (18)$$

has the solution

$$\tilde{\rho}(t) = \exp(t\tilde{\mathcal{L}})\tilde{\rho}(0), \quad (19)$$

where

$$\begin{aligned} \tilde{\mathcal{L}} = & -(1-\omega)i(I_N \otimes H - H^T \otimes I_N) \\ & + \omega \sum_{k \in G}^K (L_k^* \otimes L_k - \frac{1}{2}(I_N \otimes L_k^\dagger L_k + L_k^T L_k^* \otimes I_N)) \\ & + \sum_{k \in G_\Gamma} \Gamma_k (L_k^* \otimes L_k - \frac{1}{2}(I_N \otimes L_k^\dagger L_k + L_k^T L_k^* \otimes I_N)) \\ & + \sum_{k \in G_\Theta} \Theta_k (L_k^* \otimes L_k - \frac{1}{2}(I_N \otimes L_k^\dagger L_k + L_k^T L_k^* \otimes I_N)) \end{aligned} \quad (20)$$

and $\rho(t)$ is related to $\tilde{\rho}(t)$ by the mapping $\tilde{\rho}_k \longleftrightarrow \rho_{ij}$. $\tilde{\mathcal{L}}$ is referred to as a ‘super-operator’ as its action on an operator returns another operator.

3. Computational Methods

QSW_MPI has been developed primarily for use on distributed memory systems, computational clusters consisting of multiple networked CPUs each with their own local memory. This strategy affords a much higher degree of parallelization than is possible with a threaded model whereby multiple tasks run on the same CPU with shared memory access [16]. Parallelization was achieved using the Message Passing Interface (MPI) protocol, a well established and highly portable standard

for distributed memory computation. Essentially, MPI runs multiple copies of a given program over an *MPI communicator*, in which each process (or *node*) is identified sequentially by its *rank*. Communication occurs between these isolated nodes via the passing of messages as instructed by directives placed in code using the MPI API.

Overall, the Fortran libraries developed for QSW-MPI consist of approximately 45 subroutines comprised of over 3000 lines of code, most of which are optimized for parallel execution. This section thus provides a high level overview of approaches and design considerations used in the development of the package. We begin with a discussion of the selected matrix exponentiation methods which, by Equation 19, is the primary task at hand. This is followed by an outline of the data structures and parallelization scheme used to achieve fast and memory efficient QSW simulation.

3.1. Matrix Exponentiation

The matrix exponential is defined by a converging Taylor series

$$\exp(A) = \sum_{j=0}^{\infty} \frac{(A)^j}{j!} \quad (21)$$

where $A \in \mathbb{C}^{n \times n}$ and $\vec{u} \in \mathbb{C}^n$. Direct application of this formula is not generally practical as the rate of convergence can vary wildly. An additional challenge is that, for $A = \mathcal{L}$, n grows exponentially with \tilde{N} , meaning that multiple powers of A may not be stored easily in computer memory. For this reason, it is preferable to directly approximate $\exp(A)\vec{u}$, thus avoiding the need to store intermediate matrices [17].

Of the algorithms used to compute $\exp(A)\vec{u}$, perhaps the most common for sparse matrices are the Krylov subspace techniques. These proceed by approximating the n -dimensional problem in a smaller m -dimensional subspace of $\text{span}\{\vec{u}, A\vec{u}, \dots, A^{m-1}\vec{u}\}$, on which efficient dense matrix exponentiation methods may then be used [18].

Other popular techniques are based on polynomial expansions of $\exp(A)$. For example, the Chebyshev approximation method is based on the Chebyshev expansion of the matrix exponential about the point $[\lambda_{\min}, \lambda_{\max}] \in \mathbb{C}$, where λ_{\min} and λ_{\max} are the eigenvalues of A with the smallest and largest real values [19–21].

This method is popular in quantum simulation as it offers fast and reliable convergence for Hermitian matrices [17, 21, 22]. It also has a lower memory overhead than the Krylov methods, not requiring storage of basis vectors and ancillary matrices [18]. However, if A is non-Hermitian with eigenvalues off the negative real axis (of the complex plane), the expansion can produce a poor approximation of $\exp(A)$ [17]. This is shown in Figure 2, where complex eigenvalues resulting from inclusion of the non-unitary Lindblad operators in $\tilde{\mathcal{L}}$ result in poor numerical stability proportional to ω and t .

A third approach, ‘scaling and squaring’, takes advantage of the relationship,

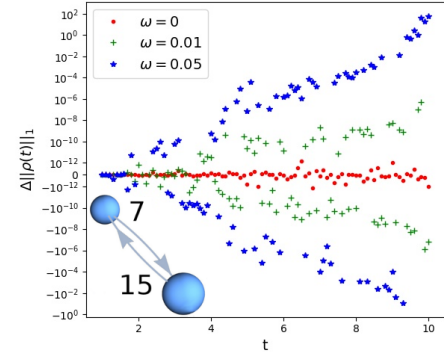


Figure 2: Norm-wise error resulting from application of the Chebyshev approximation method as given in Ref. [21] to simulate a QSW on a directed dimer graph with target numerical error less than 10^{-18} . Error was determined by comparison with the result given by the Mathematica MatrixExp function.

$$\exp(A)\vec{u} = \exp(s^{-1}A)^s \vec{u} = \left(\prod_{s \text{ times}} \exp(s^{-1}A) \right) \vec{u} = \vec{v} \quad (22)$$

to reduce the number of terms in a series expansion of $\exp(A)$ needed to satisfy a numerical error less than ϵ [23]. Let $T_m(A)$ denote a Taylor series expansion to m terms. Then,

$$\exp(A)\vec{u} \approx \left(T_m(s^{-1}A) \right)^s \vec{u} = \left(\sum_{j=0}^m \frac{s^{-1}A^j}{j!} \right)^s \vec{u}. \quad (23)$$

Historically, this method has not been favoured due to difficulties in the selection of the optimal m and s parameters [17]. However, the scaling and squaring algorithm developed by Al-Mohy and Higham [23] achieves this reliably via backwards error analysis. This method shares the advantages of the Chebyshev approximation over the Krylov methods. It has also been experimentally demonstrated as being numerically stable for both Hermitian and non-Hermitian matrices, with computational performance comparable to the Chebyshev approximation in both cases [23]. This method is also well tested; it forms the basis for sparse matrix exponentiation in the widely used SciPy Python library [24]. Despite its perceived success, there has been little explicit discussion of its use in the literature of quantum simulation. This may be due in part to it not being currently implemented in widely used parallel numerical libraries such as PetSc [25]. As such, this method has been selected for its purported advantages, stability with non-Hermitian matrices and novelty in the context of computational quantum physics.

3.2. Sparse operator representation

As all of the terms in $\tilde{\mathcal{L}}$ involve a Kronecker product with an identity matrix or sparse Lindblad operator, $\tilde{\mathcal{L}}$ is highly sparse. In fact, while the total number of matrix elements in \mathcal{L} is \tilde{N}^4 , the number of non-zero entries is of the order \tilde{N}^3 . This means that there is a sparsity of over 90% for graphs with 20 vertices or greater. Therefore, the scope of possible simulations can be greatly increased by representing $\tilde{\mathcal{L}}$ using a sparse matrix for-

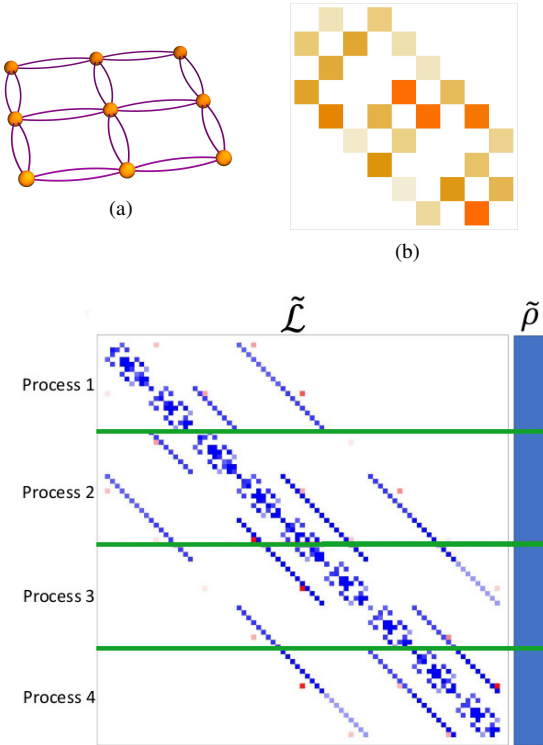


Figure 3: A directed square lattice graph with an adjacency matrix, G , of non-zero structure as shown in (b). The orange squares denote the relative magnitude of each value. In (c) the non-zero structure of the resulting QSW superoperator, \tilde{L} , with $\omega = 0.5$. Red and blue intensity depicts the relative magnitude of the non-zero values, with red denoting a real valued entry and blue denoting a complex valued entry. Green vertical lines depict the parallel row-wise partitioning of \tilde{L} and the vectorized density operator, $\tilde{\rho}$, for a MPI communicator consisting of four nodes.

mat. For this, the Compressed Sparse Rows (CSR) format has been selected. An advantageous property of the CSR datatype is that it provides for the efficient access of matrix rows, as each row has its non-zero column indices and values stored as a contiguous sub-array. This quality distinguishes CSR from other common sparse matrix formats and allows for the efficient computation of matrix-vector products: the fundamental algebraic operation in matrix exponentiation.

3.3. Parallel Partitioning Scheme

The structure of \tilde{L} resulting from a directed lattice graph is shown in Figure 3. It displays a high degree of structural symmetry, with a block-circulant structure along its diagonal flanked by diagonal striping. However, it is important to note that, aside from the case of $\omega = \Gamma_k = \Theta_k = 0$, \tilde{L} is not block circulant as generally $L_{ij} \neq L_{ji}$. Hence, efficient eigendecomposition techniques, which take advantage of analytical solutions for the eigenvalues and eigenvectors of circulant block matrices, do not provide a general method for obtaining $\rho(\tilde{t})$ [26].

Despite this, these structural properties are easily exploited. Firstly, the diagonal structure results in each row being primarily dependant during matrix-vector multiplication on vector elements within the ‘vicinity’ of its row index. This motivates

adoption of the row-wise partitioning scheme depicted in Figure 3. This ensures that the parallel processes communicate primarily with nodes containing vector elements adjacent to their local partition, thus limiting inter-process communication.

Secondly, the block structure of \tilde{L} means that the superoperator can be efficiently constructed directly from the CSR representations of H and $L = \sum_k^{\tilde{N}} L_k = \sqrt{M_{ij}}$, avoiding the need to form intermediate Kronecker products or store each Lindblad operator separately. With this approach, the construction of \tilde{L} is independent at each node following receipt of G , and \tilde{L} is consistently stored in distributed memory.

As $\exp(A)\vec{u}$ is found through repeated action of A on a vector, MPI inter-process communication in each multiplication cycle is further reduced by the determination of the specific vector elements that need to be sent and received with each multiplication on formation of \tilde{L} . This has the additional benefit of ensuring that the sparse matrix multiplication algorithm implemented in QSW_MPI acts on contiguous row sub-arrays of the CSR values and column index arrays, as is typically the case for non-parallel sparse matrix multiplication [27].

4. Package Overview

The QSW_MPI software package brings together the computational methods described in Section 3 through a Python interface, thus providing a user friendly means of high performance QSW simulation. This also provides additional support for the storage, analysis and basic visualization of the simulation results using external Python packages. While targeted towards distributed memory systems, QSW_MPI is highly portable due to its minimal dependence on external parallel libraries such as PetSc, which may require significant user configuration. It may be compiled on any system with an MPI implementation, HDF5 file format support, and a recent Python installation [25].

The extra functionality provided by the Python interface is built on the widely supported NumPy, SciPy, NetworkX, Matplotlib, MPI for Python and h5Py packages. NumPy and SciPy are numerical libraries which are used in QSW_MPI to interface with the Fortran subroutines and provide in-python support for the CSR datatype [24, 28]. NetworkX provides a rich environment for the construction and analysis of networks [29]. It is used in conjunction with Matplotlib to provide basic support for the visualization of simulation results, and the structure of networks is augmented with sources and sinks [30]. MPI for Python provides Python support for MPI directives and the passing of MPI communicator handles between the Python interface and Fortran subroutines [31–33].

A complete explanation of the methods contained in QSW_MPI exceeds the scope of this document, further documentation and installation instructions are included with the package and are additionally hosted on Read the Docs [34]. This section provides usage examples which demonstrate the most significant features of QSW_MPI and typical simulation workflows.

4.1. Usage Example

4.1.1. Basic QSW simulation

As MPI based programs are parallelized through running multiple instances of the same program, they do not support the use of interactive environments such as the Jupyter notebook. The following code is to be placed in ‘example.py’, which is then run by issuing the terminal command:

```
mpirun -N n python example.py
```

where n is a user specified parameter equal to the number of MPI nodes. Another possible workflow is to save the simulation results to disc and carry out visualization and analysis interactively using the QSW_MPI python modules, exclusive of MPI.py. Steps necessary to achieve this are covered in Section 4.1.2.

In this example a QSW is simulated on a directed wheel graph, shown in Figure 4 (a). First, import the required modules:

```
from mpi4py import MPI
import qsw_mpi as qsw
import numpy as np
import networkx as nx
```

Next, set up the MPI environment. This involves creating an MPI communicator object and defining the process rank:

```
mpi_comm = MPI.COMM_WORLD
rank = mpi_comm.Get_rank()
```

For this example, Networkx is used to create a wheel graph at each rank. The graph is then converted to a SciPy CSR matrix:

```
vertices = 4
Graph = nx.wheel_graph(vertices)
G = nx.to_scipy_sparse_matrix(Graph,
    dtype=np.complex128)
```

and made directed by assigning random weights between $(0, 1]$ to the edges of G . Note the use of $\text{np.random.seed}(1)$: it ensures that each MPI process generates the same sequence of random numbers:

```
np.random.seed(1)
for i in range(G.count_nonzero()):
    G.data[i] = G.data[i]*np.random.random()
```

From G , a directed Laplacian is constructed as per Equation 4. This is used to obtain the Lindblad matrix and then symmetrised to obtain the Hamiltonian as defined by Equation 11:

```
gamma = 1
H = qsw.operators.graph(gamma, G)
L = qsw.operators.site_lindblads(H)
qsw.operators.symmetrise(H)
```

A walk object is then instantiated; upon creation, it constructs the distributed super-operator \mathcal{L} and determines its 1-norm power series.

```
omega = 0.1
wheel_graph = qsw.MPI.walk(
    omega, H,
    L, mpi_comm)
```

The initial state of the walker, $\rho(0)$, is then defined and passed to the walk object which vectorizes and partitions the density matrix over the MPI communicator. Note that Python is 0-indexed, meaning that the below code specifies an initial state of $\rho(0) = |1\rangle\langle 1|$ as per Equation 6.

```
rho_0 = np.zeros(
    G.shape,
    dtype=np.complex128)
rho_0[0,0] = 1
wheel_graph.initial_state(rho_0)
```

A single time point is obtained through use of the ‘step’ method. ‘target’ defines the rank to which the $\rho(t)$ will be returned.

```
t = 5
rho_t = wheel_graph.step(5, target = 0)
```

A time series is obtainable using the ‘series’ method.

```
t1 = 0
t2 = 5
steps = 50
rho_t_series = wheel_graph.series(
    t1, t2,
    steps,
    target=0)
```

To analyse the results, it is essential to act on ‘rho_t’ and ‘rho_t_series’ from the target rank: they will not be defined elsewhere. This is achieved by simply enclosing these tasks in an ‘if’ statement which checks that the process rank is equal to the target rank. Analysis may proceed by acting directly on the ‘rho_t’ and ‘rho_t_series’ numpy arrays, or through use of the QSW_MPI measurements sub-module. For example, the vertex populations are obtained by

```
if rank == 0:
    pop_step = qsw.measure.populations(
        rho=rho_t)
    pop_series = qsw.measure.populations(
        rho=rho_t_series)
```

where, as expected, the last element of ‘pop_series’ is equal to ‘pop_step’ and the populations at each time-step sum to 1.

```
print(pop_step)
print(pop_series[50])
print(np.sum(pop_step))
```

```
[0.25851439 0.17227131 0.427752  0.1414623 ]
[0.25851439 0.17227131 0.427752  0.1414623 ]
0.999999999999978
```

Inter-vertex coherence can likewise be extracted with the coherences method. The obtained population and coherence measurements are shown in Figures 4 (c) and (d). These plots can be reproduced with use of the ‘population_lines’ and ‘coherence_lines’ methods provided in the `qsw_mpi.plot` module.

```
vertex_pairs, coh = \
qsw.measure.coherences(rho=rho_t_series)
```

Using this ‘walk’ object, multiple simulations may be carried out with different $\rho(0)$ and values of ω . QSW_MPI supports a small number of default initial states; for example, ‘even’ creates $\rho(0)$ in an equal superposition across all vertices.

```
wheel_graph.initial_state('even')
wheel_graph.set_omega(0.5)
```

4.1.2. Introducing Dissipators

This model can now be expanded to include absorption and emission processes, with the connection of ‘sources’ and ‘sinks’ to the graph following the conventions defined in Equations 14 and 15. These are described by tuples of two NumPy arrays, the first giving the point of connection and the second the absorption or emission rates at those vertices, noting again that Python is 0-indexed.

```
sources = ([0], [0.7])
sinks = ([3], [0.8])
```

The resulting graph is shown in Figure 5 (a). As these additions result in a structural change in H and L , it is necessary to create a new walk object.

```
wheel_graph_augmented = qsw.MPI.walk(
    omega, H,
    L, mpi_comm,
    sources = sources,
    sinks = sinks)
```

When running a simulation either remotely or for a large system, it is more convenient to save the output directly to disc. To do so, first create a .qsw file to contain the results of walk carried out using the ‘wheel_graph_augmented’ object. This walk makes use of another default initial state: ‘sources’, which distributes $\rho(0)$ over all defined source vertices. The ‘chunk_size’ parameter controls the number of time-steps between each write to disc. By default, chunked saving is automatically enabled for series with an estimated output size greater than 4 GB.

```
wheel_graph_augmented.File(
    'usage_example',
    action = "w")
wheel_graph_augmented.initial_state('sources')
wheel_graph_augmented = qsw.MPI.walk(
    omega, H, L, mpi_comm,
    sources = sources,
    sinks = sinks)
wheel_graph_augmented.series(
```

```
t1, t2,
steps, save = True,
name = "series 1"
chunk_size = 5)
```

Vertex populations and coherences can be extracted directly from the .qsw file, thus avoiding the need to load the entire series into memory. The results as shown in Figure 5 (b) and (c). With a higher number of vertices an extra plotting dimension can add some clarity. These plots can be reproduced via the ‘population_bars’ and ‘coherence_bars’ methods provided in the `qsw_mpi.plot` module.

```
if rank == 0:
    file = qsw.io.File('usage_example')
    pop_series = qsw.measure.populations(
        rho=rhot)
    vertices_pairs, coh = qsw.measure.coherences(
        rho=rho_t_series)
```

Later, further simulations with the same system can be conducted by initializing ‘wheel_graph_augmented’ using the ‘usage_example.qsw’ which contains all of the arrays necessary to reconstruct the same super-operator and a record of the $\rho(0)$ used for saved walks.

```
wheel_graph_augmented.File(
    omega,
    'usage_example',
    mpi_comm)
```

5. Validation and Performance

The following tests were performed on four sets of graphs generated via Networkx. These included a set of line graphs, square lattice grids and a random graph with $n \log(n)$ edges with 4 to 4096 vertices. This corresponded to a maximum \tilde{L} size of approximately 16.5×16.5 million. The final set consisted of fully connected dense graphs ranging from 4 to 441 vertices. In each case the graph edges were assigned a random edge weighting in the interval (0,1].

Figure 6 shows a comparison of results obtained using QSW_MPI and the Mathematica package QSWalk.m, which relies on the Mathematica MatrixExp function for walk propagation [10]. For graphs with 100 vertices taken from the above sets, the scaling and squaring algorithm achieved the specified target precision over an interval containing 1000 time-steps, as shown in Figure 6. As an additional check, the populations of $\rho(t)$ were totalled for each returned result during the overall benchmarking process. Norm preservation was consistently observed within the limits of the target precision.

The package performs well compared to available desktop alternatives when run on the same consumer-level hardware. As QSW_MPI, QSWalk.m and QSWalk.jl make use of sparse libraries, performance should ideally scale with the number of non-zeros rather than the size of \tilde{L} [10, 11]. This is shown in Figure 7, where for the line, square grid and random graph sets,

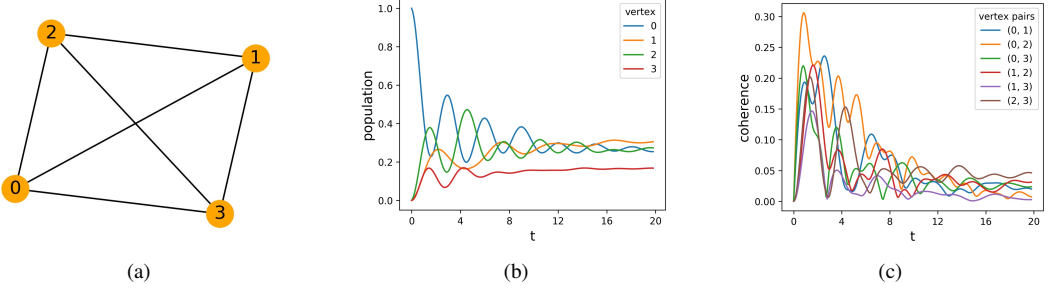


Figure 4: The vertex populations for a QSW on the 4 vertex star graph (a) are shown in (b) and its inter-vertex coherence in (c).

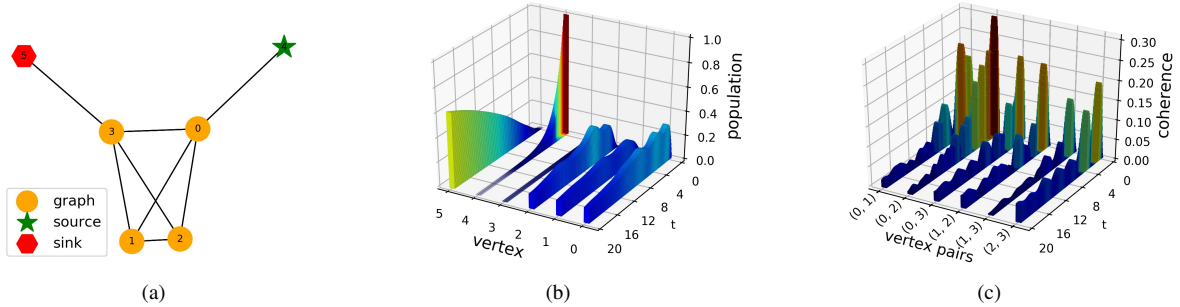


Figure 5: The same graph as in Figure 4 with an absorption site at vertex 0 and emission site at vertex 3 is shown in (a), with the vertex populations for a QSW over the same period shown in (b) and the inter-vertex coherence in (c). Note the exponential decay of population at the source vertex 4 and its accumulation at sink vertex 5 over the duration of the walk.

QSW_MPI is clearly the fastest option. This is due in part to the higher memory efficiency afforded by $\tilde{\mathcal{L}}$ construction method used by QSW_MPI. In Figure 7 (b), QSWWalk.jl deviates from linear scaling at approximately 1×10^6 non-zeros as it begins to access on disc swap space. At that point, it requires ~ 40 s to generate $\tilde{\mathcal{L}}$ as opposed to the ~ 0.6 s needed by QSW_MPI. The same effect is observed in Figure 7 (c) for QSW_MPI where, at approximately 4.5×10^7 non-zeros, QSW_MPI deviates from linear scaling. However, this occurs far later than with the other two packages. As shown in Figure 7 (d), QSWWalk.jl is the best performer for the case of complete graphs. Parallel operations in QSW_MPI are least efficient in this instance as each row of $\tilde{\mathcal{L}}$ has the highest possible number of row elements meaning that the partitioning scheme has the highest possible MPI inter-process connectivity. In addition, QSWWalk.jl utilizes a matrix exponentiation module which is able to switch to dense matrix multiplication methods given a sufficient number of non-zeros [11]. However, the scalability of QSW_MPI means that it is capable of higher performance with a modest increase in the number of available CPU cores.

This is confirmed by tests run on the Pawsey Supercomputing Centre’s Magnus system [35], where QSW_MPI is observed to scale well with the number of CPU cores, as shown in Figure 8. With use of Amdahl’s law as an approximate measure of the total parallelism, the proportion of parallel operations for the line, square grid, random graph and complete graph were 0.96, 0.91, 0.88 and 0.85. Unsurprisingly, parallelism is highest for

the line graph, for which there is the lowest number of elements per row in $\tilde{\mathcal{L}}$. The case of complete graphs serves as a measure of the lower bound of QSW_MPI performance.

6. Conclusion

Quantum systems often feature a large number of degrees of freedom, to which the size of their Hilbert space has an exponential relationship. The main challenge of developing QSW_MPI was to successfully utilize memory and processor efficient methods from the field of high performance computing to render the simulation of such systems practical on currently available hardware. An additional challenge arose in non-Hermitian structure of super-operator of the quantum stochastic walk model: methods common to most quantum simulations were not directly applicable as they were unstable with respect to the non-unitary dynamics.

These challenges were overcome by use of the Message Passing Interface standard of distributed computing to develop an implementation of a relatively recent method of matrix exponentiation, stable for both Hermitian and non-Hermitian matrices. As far as we know, this is the first implementation of this specific algorithm in the context of distributed memory computing. In order to ensure memory efficiency, sparse data-structures were employed in the creation of the necessary operator matrices and during basic linear algebra operations. This resulted in software which out-performs existing packages to

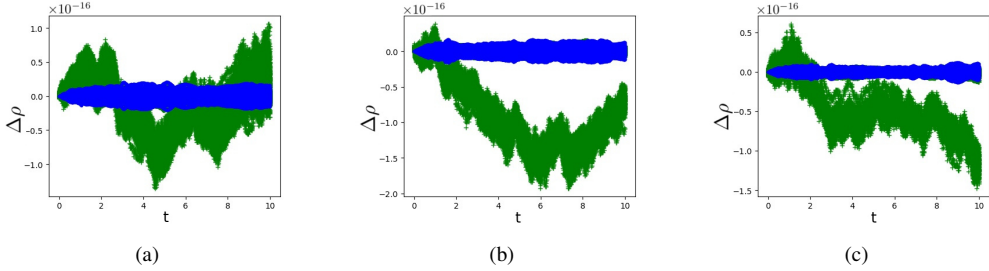


Figure 6: Difference between results calculated to double precision using QSW_MPI and QSWalk.m. Green and blue denotes the real and imaginary components of $\rho(t)_{ij}$ respectively. Each walk was carried out on a graph of 100 vertices for $\omega = 0.1$, $t = [0, 10]$ and $q = 1000$. (a) Line graph, (b) Square Lattice and (c) Random graph.

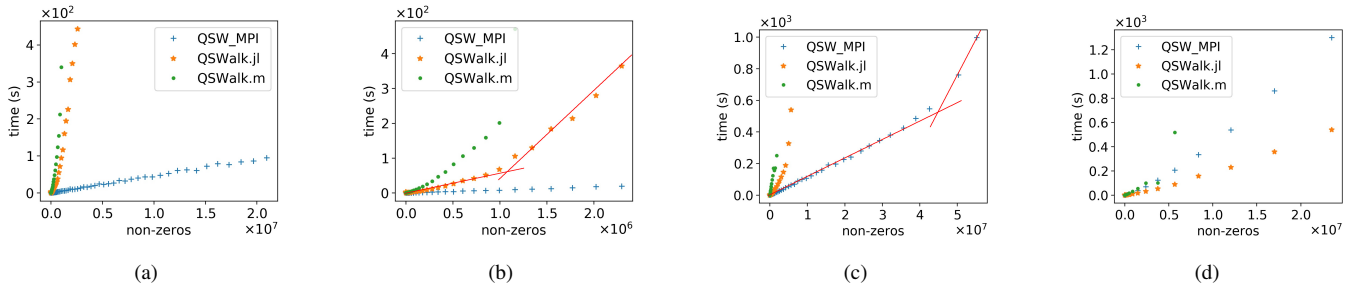


Figure 7: Performance of QSW simulation packages on a desktop computer. For all walks $\omega = 0.1$ and $t = 10$. The QSWalk.jl and QSWalk.m packages consist of single-threaded programs, while QSW_MPI running with four MPI nodes (one for each available CPU core). (a) shows performance on the set of line graphs, (b) square grid graphs, (c) random graphs with $n \log(n)$ edges and (d) complete graphs. System specifications: Intel i7-6700K 4 cores at 4.0 GHz and 16 GB RAM at 3200 MHz. The red lines in sub-figures (b) and (c) highlight a change in the scaling of the corresponding package due to a transition from in RAM to RAM + disc storage.

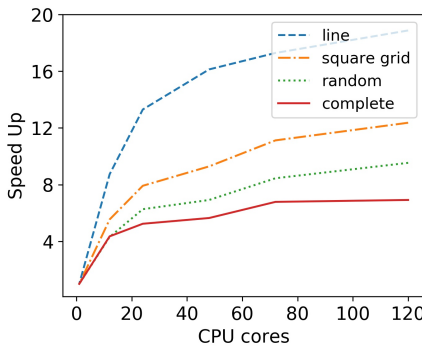


Figure 8: Proportional speedup as a function of CPU cores for QSW_MPI running on the Pawsey Supercomputing Center's Magnus system. Line graph, 4096 vertices. Square Lattice 4096 vertices. Random graph, 2209 vertices. Complete graph, 196 vertices. System specifications: XC40 Series Supercomputer, 2 × Intel Xeon E5-2690V3 12 cores at 2.6 Ghz and 64 GB RAM per node.

the extent of many thousands of basis states when simulating sparsely connected systems, on both distributed supercomputer clusters and readily available consumer computers. Key to this performance increase was the detailed analysis of the structure of the vectorized quantum stochastic walk super-operator. While somewhat mundane from a theoretical or technical standpoint, the resulting performance highlights the value of ‘tailor-

made’ approaches compared to use of ‘off the shelf’ software libraries when simulating extensive systems.

As QSW_MPI implements its own basic linear algebra subroutines, its parallel performance may not be optimal as compared to an implementation utilising pre-existing parallel libraries such as PetSc. However, the installation of such libraries is not always straightforward; thus QSW_MPI, easily installed from the Python PyPI package repository and dependent only on packages included on most Unix-based operating systems, gains a good deal of portability due to this omission. Nevertheless, it would be beneficial to extend this package to allow for the use of external linear algebra libraries as a user-specified compile time option. This would be relatively easy to achieve due to the modularity of the package’s underlying Fortran libraries.

In its relatively short period of existence, the quantum stochastic walk model has proven to be highly versatile. Release of the QSW_MPI package to the research community increase its scope to the study of larger and more expressive systems.

Ackowlegements

This work was supported by the Muriel and Colin Ramm Postgraduate Scholarship in Physics, and resources provided by the Pawsey Supercomputing Centre with funding from the Australian Government and the Government of Western Australia.

References

[1] E. Matwiejew, QSW_MPI (Mar. 2020). doi:10.5281/zenodo.3697336.

[2] Q. Zhang, C. Zhang, L. Cao, Z. Wang, B. An, Z. Lin, R. Huang, Z. Zhang, C. Wang, W. Lin, Frster Energy Transport in MetalOrganic Frameworks Is Beyond Step-by-Step Hopping, *Journal of the American Chemical Society* 138 (16) (2016) 5308–5315. doi:10.1021/jacs.6b01345.

[3] O. Milken, A. Blumen, Continuous-time quantum walks: Models for coherent transport on complex networks, *Physics Reports* 502 (2) (2011) 37–87. doi:10.1016/j.physrep.2011.01.002.

[4] L. C. G. Govia, B. G. Taketani, P. K. Schuhmacher, F. K. Wilhelm, Quantum simulation of a quantum stochastic walk, *Quantum Science and Technology* 2 (1) (2017) 015002. doi:10.1088/2058-9565/aa540b.

[5] H. Tang, Z. Feng, Y.-H. Wang, P.-C. Lai, C.-Y. Wang, Z.-Y. Ye, C.-K. Wang, Z.-Y. Shi, T.-Y. Wang, Y. Chen, J. Gao, X.-M. Jin, Experimental Quantum Stochastic Walks Simulating Associative Memory of Hopfield Neural Networks, *Physical Review Applied* 11 (2) (2019) 024020. doi:10.1103/PhysRevApplied.11.024020.

[6] E. Snchez-Burillo, J. Duch, J. Gmez-Gardees, D. Zueco, Quantum Navigation and Ranking in Complex Networks, *Scientific Reports* 2 (2012) 605. doi:10.1038/srep00605.

[7] T. Loke, J. W. Tang, J. Rodriguez, M. Small, J. B. Wang, Comparing classical and quantum PageRanks, arXiv:1511.04823 [physics, physics:quant-ph]ArXiv: 1511.04823.

[8] M. Mohseni, P. Rebentrost, S. Lloyd, A. Aspuru-Guzik, Environment-assisted quantum walks in photosynthetic energy transfer, *The Journal of Chemical Physics* 129 (17) (2008) 174106. doi:10.1063/1.3002335.

[9] P. Schijven, Quantum stochastic walks : a model for coherent and incoherent transport on networks, Ph.D. thesis (Jan. 2014).

[10] P. E. Falloon, J. Rodriguez, J. B. Wang, QSWalk: a Mathematica package for quantum stochastic walks on arbitrary graphs, *Computer Physics Communications* 217 (2017) 162–170. doi:10.1016/j.cpc.2017.03.014.

[11] A. Glos, J. A. Miszcza, M. Ostaszewski, QSWalk.jl: Julia package for quantum stochastic walks analysis, *Computer Physics Communications* 235 (2019) 414–421, arXiv: 1801.01294. doi:10.1016/j.cpc.2018.09.001.

[12] P. E. Falloon, J. B. Wang, Reply to Glos et al. [arXiv:1801.01294] on QSWalk.m package performance, arXiv:1903.01323 [quant-ph]ArXiv: 1903.01323. URL <http://arxiv.org/abs/1903.01323>

[13] N. G. Kampen, *Stochastic Processes in Physics and Chemistry*, Elsevier, 2007. doi:10.1016/B978-0-444-52965-7.X5000-4.

[14] H.-P. Breuer, F. Petruccione, *The theory of open quantum systems*, nachdr. Edition, Clarendon Press, Oxford, 2009, oCLC: 553486996.

[15] J. D. Whitfield, C. A. Rodriguez-Rosario, A. Aspuru-Guzik, Quantum stochastic walks: A generalization of classical random walks and quantum walks, *Physical Review A* 81 (2). doi:10.1103/PhysRevA.81.022323.

[16] MPI Forum.

[17] C. Moler, C. Van Loan, Nineteen Dubious Ways to Compute the Exponential of a Matrix, Twenty-Five Years Later, *SIAM Review* 45 (1) (2003) 3–49. doi:10.1137/S00361445024180.

[18] B. N. Sheehan, Y. Saad, R. B. Sidje, Computing the matrix exponential with laguerre polynomials, *Electronic Transactions on Numerical Analysis* 37 (2010) 147–165.

[19] J. B. Wang, T. T. Scholz, Time-dependent approach to scattering by chebyshev-polynomial expansion and the fast-fourier-transform algorithm, *Physical Review A* 57 (1998) 3554.

[20] S. Midgley, J. B. Wang, Complex absorbing potential and chebyshev propagation scheme, *Physical Review E* 61 (2000) 920.

[21] J. A. Izaac, J. B. Wang, *Computational Quantum Mechanics*, Springer Nature, Switzerland, 2018.

[22] J. A. Izaac, J. B. Wang, pyCTQW: A continuous-time quantum walk simulator on distributed memory computers, *Computer Physics Communications* 186 (2015) 81–92. doi:10.1016/j.cpc.2014.09.011.

[23] A. Al-Mohy, N. Higham, Computing the Action of the Matrix Exponential, with an Application to Exponential Integrators, *SIAM Journal on Scientific Computing* 33 (2) (2011) 488–511. doi:10.1137/100788860.

[24] E. Jones, T. Oliphant, P. Peterson, SciPy: Open source scientific tools for Python (2001). URL <http://www.scipy.org/>

[25] S. Balay, S. Abhyankar, M. F. Adams, J. Brown, P. Brune, K. Buschelman, L. Dalcin, A. Dener, V. Eijkhout, W. D. Gropp, D. Karpeyev, D. Kaushik, M. G. Knepley, D. A. May, L. C. McInnes, R. T. Mills, T. Munson, K. Rupp, P. Sanan, B. F. Smith, S. Zampini, H. Zhang, H. Zhang, PETSc Web page, 2019.

[26] S. Rjasanow, Effective algorithms with circulant-block matrices, *Linear Algebra and its Applications* 202 (1994) 55–69. doi:10.1016/0024-3795(94)90184-8.

[27] J. V. Kepner, J. R. Gilbert, *Graph algorithms in the language of linear algebra*, Software, environments, and tools, Society for Industrial and Applied Mathematics, Philadelphia, 2011.

[28] T. Oliphant, *NumPy: A guide to NumPy*, 2006, published: USA: Trelgol Publishing.

[29] A. A. Hagberg, D. A. Schult, P. J. Swart, Exploring Network Structure, Dynamics, and Function using NetworkX, in: G. Varoquaux, T. Vaught, J. Millman (Eds.), *Proceedings of the 7th Python in Science Conference*, Pasadena, CA USA, 2008, pp. 11 – 15.

[30] J. D. Hunter, *Matplotlib: A 2d graphics environment*, *Computing in Science & Engineering* 9 (3) (2007) 90–95. doi:10.1109/MCSE.2007.55.

[31] L. Dalcin, R. Paz, M. Storti, MPI for Python, *Journal of Parallel and Distributed Computing* 65 (9) (2005) 1108–1115. doi:10.1016/j.jpdc.2005.03.010.

[32] L. Dalcin, R. Paz, M. Storti, J. DEla, MPI for Python: Performance improvements and MPI-2 extensions, *Journal of Parallel and Distributed Computing* 68 (5) (2008) 655–662. doi:10.1016/j.jpdc.2007.09.005.

[33] L. D. Dalcin, R. R. Paz, P. A. Kler, A. Cosimo, Parallel distributed computing using Python, *Advances in Water Resources* 34 (9) (2011) 1124–1139. doi:10.1016/j.advwatres.2011.04.013.

[34] E. Matwiejew, QSW_MPI documentation (2020). URL <https://qsw-mpi.readthedocs.io>

[35] The Pawsey Supercomputing Centre. URL <https://www.pawsey.org.au/>